Journal of *Marine Science and Engineering*

MDPI

Article

ANFIS-Based Course Controller Using MMG Maneuvering Model

Yu Guo [1], Rui Yang [1], Zhiheng Zhang [1,*] and Bing Han [2]

[1] Merchant Marine College, Shanghai Maritime University, Shanghai 201306, China; yuguo@shmtu.edu.cn (Y.G.); 202330110258@shmtu.edu.cn (R.Y.)
[2] Shanghai Ship and Shipping Research Institute Co., Ltd., Shanghai 200135, China; han.bing@coscoshipping.com
* Correspondence: zhzhang@shmtu.edu.cn

Abstract: In the domain of course control, traditional methods such as proportional–integral–derivative (PID) control often exhibit limitations when addressing complex nonlinear systems and uncertain disturbances. To mitigate these challenges, the adaptive neuro-fuzzy inference system (ANFIS) has been integrated into course control strategies. The primary objective of this study is to investigate the course control characteristics of vessels governed by the ANFIS controller under both normal and severe sea conditions. A three-degree-of-freedom (3-DOF) maneuvering model set (MMG) was employed and validated through sea turning tests. The design of the ANFIS controller involved a combination of the backpropagation algorithm with the least square method. Training data for the ANFIS control system were derived from a linear control framework, followed by simulation tests conducted under normal and severe sea conditions to assess control performance. The simulation results indicate that in normal sea conditions, ANFIS has more stable heading control (smaller A_ψ), but at the cost of more energy consumption (larger I_δ). Notably, response time is reduced by approximately 36.7% compared to that of the linear controller. Conversely, during severe sea conditions, ANFIS exhibits an increase in response time by about 33.3% relative to the linear controller while maintaining a smaller I_δ. In the whole course control stage, the stability is better than the linear controller, and it has better energy-saving characteristics. Under scenarios involving small and large course alterations, A_ψ values for ANFIS are approximately 11.28% and 13.97% higher than those observed with the best-performing linear controller ($\lambda_\psi = 60$), respectively. As the propeller speed increases, the A_ψ value of the ANFIS controller decreases significantly, to about 62.71%, indicating that the energy efficiency is improved and the course stability is also enhanced. In conclusion, it can be asserted that the implementation of an ANFIS controller yields commendable performance in terms of controlling vessel courses effectively.

Keywords: heading control; ANFIS; MMG model; simulation

check for updates

Academic Editor: Zaojian Zou

Received: 20 January 2025
Revised: 27 February 2025
Accepted: 28 February 2025
Published: 1 March 2025

Citation: Guo, Y.; Yang, R.; Zhang, Z.; Han, B. ANFIS-Based Course Controller Using MMG Maneuvering Model. *J. Mar. Sci. Eng.* **2025**, *13*, 490. https://doi.org/10.3390/jmse13030490

Copyright: © 2025 by the authors. Licensee MDPI, Basel, Switzerland. This article is an open access article distributed under the terms and conditions of the Creative Commons Attribution (CC BY) license (https://creativecommons.org/licenses/by/4.0/).

1. Introduction

Maritime transport safety has become an important factor restricting the rapid development of the shipping industry [1]. In addition to the burning process of the ship's main engine and auxiliary engine, a large number of pollutants will be produced, affecting the safety of maritime transportation [2]. Ship course control is also the main content of maritime transportation security, and the intelligent development of control systems is the main trend of navigation technology development. For ocean-going ships, course control is essential to enhance maritime traffic safety, especially in the era of autonomous ships [3].

The traditional controller is considered an effective way to realize ship course keeping. The common method is proportional–integral–differential (PID) control. Mochammad S

et al. [4] proposed a ship control system using a PID controller, realized the parameter identification algorithm of the control system based on gradient approximation, and achieved good ship maneuverability. Sutulo S et al. [5] proposed a conventional PID controller for course keeping. In the range of water depth, lateral distance, and speed, the hydrodynamic interaction and maneuvering speed response of two ships during overtaking are simulated. When the ratio of water depth to the ship's draft depth is less than 2.0, the PID controller is still effective for overtaking boats. Bayezit L et al. [6] proposed a strategically coupled system based on a sensor model and PID controller for course angle control to understand the motion dynamics of ocean vessels and demonstrated the practical feasibility of the system through the "vehicle in the loop" test, demonstrating its potential to improve the efficiency of recreational ocean navigation.

Conventional PID controllers are not robust to external interference, in contrast to fraction-order controllers, sigmoid PID controllers, BELBIC PID controllers, and multi-node hormone neuroendocrine PID controller, which have received attention. Liu L et al. [7] proposed an FOPID controller based on the three-dimensional stable region analysis method, which improved the robustness of the title control of unmanned ships. Although the robustness of the controller has been improved to some extent, the complexity of determining the parameters of the FOPID controller results in a long control response time, which is obviously insufficient in the face of transient title control situations. Suid MH et al. [8] proposed the parameters of the SPID controller obtained using an enhanced self-tuning heuristic optimization method called the nonlinear sine-cosine algorithm (NSCA) to achieve a better dynamic response. TAO S et al. [9] used (BELBIC PID) to control the heading of autonomous ground vehicles. Then, in order to achieve better path tracking performance and drive stability, the PSO algorithm was used to optimize the parameters, and the results were good. To sum up, the PID controller has the characteristics of a simple structure in the control field, but it needs manual adjustment of parameters and has poor adaptability.

In order to improve the shortcomings of PID control, robust controllers are introduced into this topic. Muzammal M et al. [10] proposed nonlinear control algorithms based on variable structure, namely integral sliding mode, double integral sliding mode, terminal sliding mode, and super spiral sliding mode controller. The controller switches between different control laws depending on the system state, ensuring robust performance in different sea conditions. Hosseinabadi P et al. [11] designed a new finite-time robust controller for ship heading (heading) control systems with unknown mismatched external disturbances and uncertainties. A fuzzy adaptive finite time sliding mode control (FAFSMC) scheme is proposed. By combining the concept of fuzzy controller, adaptive time stability, and sliding mode control (SMC) scheme, the advantages of these two schemes are utilized and the shortcomings of single applications are compensated. Rezaei A et al. [12] designed an adaptive fractional-order sliding mode controller (AFOSMC) to reduce the adverse effects of ship roll motion. Through this adaptive control method, the designed controller is robust to the ship's lateral motion mechanics and the uncertain parameters in the fin actuator. Xu Y et al. [13] designed a global fast terminal synovial controller to track and compensate ship heave motion data. The results show that the tracking compensation effect of the improved sliding mode controller is better than that of the traditional PID control, and the tracking error is smaller than that of the traditional PID control when the improved sliding mode controller is introduced. Global fast terminal sliding mode control has good robustness and can be used in a ship heave compensation system. To sum up, the course control accuracy and stability of the robust controller are stronger, but it lacks intelligence.

In the current field of course control, in order to assist ship driving more safely, effectively reduce the danger to the crew, and improve the efficiency of maritime traffic [14], intelligent controllers are widely concerned. Both artificial neural network control and

fuzzy control belong to intelligent control. NIM N et al. [15] developed a nonlinear autoregressive model based on a neural network by combining an artificial neural network with fuzzy logic control. The results show that the two-wheeled wheelchair system combining fuzzy logic control and a neural network can improve the stability and performance. Aghaseyedabdollah M et al. [16] proposed a fuzzy adaptive synovial control scheme for cable robots. In the proposed scheme, the intelligent method is combined with the traditional synovial control to achieve the optimal adjustment of control parameters. Arifi A et al. [17] proposed an ASP modeling and control method based on Takagi–Sugeno (TS) and successfully implemented the method for carbon removal. The results show the effectiveness and superiority of the proposed control method based on TS fuzzy for dealing with complex and nonlinear biochemical processes. Han B et al. [18] proposed an improved fuzzy control method based on the integrated line-of-sight (ILOS) guidance principle in order to meet the needs of autonomous navigation and high-precision ship trajectory control. Simulation results show that the algorithm has good following performance and can maintain smooth rudder angle output. The research results provide a reference for ship path tracking control. Li Y et al. [19] proposed a berthing decision method for very large ships based on fuzzy logic. The research results provide theoretical and practical insights for the development of human-like decision-making methods for autonomous navigation in port waters and maritime safety management in the shipping industry. The model can also be further applied to develop more widely applicable autonomous navigation decision systems in narrow waters. Du L et al. [20] proposed a model combining a computational fluid dynamics solver (ANN) to calibrate the efficiency and precision weights in high-dimensional problems of ship resistance optimization. The adaptive mechanism of the model reduced the calculation cost from 1638 min to 456 min, and the optimization efficiency increased by 72.16%. The results show that the proposed adaptive mechanism can dynamically rebalance the efficiency and accuracy of the framework and provide theoretical and technical support for ship design optimization. Unar S et al. [21] proposed an artificial neural network controller for course and position control systems and selected a mathematical model with four effective thrusters to test the performance of the proposed controller. Rohit D et al. [22] proposed a deep Q-learning method based on an artificial neural network to solve the ship heading control problem. This method can make optimal decisions based on sufficient learning experience and realize the interaction between the numerical model and waypoint tracking. Wakita K et al. [23] proposed a system identification method using recurrent neural networks and free-running model testing to generate a low-speed maneuvering model, paying special attention to low-speed maneuvering in the last stage of berthing, so as to achieve automatic berthing course control. The results show that this method can accurately represent the low-speed motion of the ship. Bouaiss O et al. [24] proposed a novel nested control strategy based on adaptive radial basis function neural networks (RBFNNs) and embedded integrators (IBS) for neural network supervised control to reduce modeling uncertainty, perceived noise, and external bounded interference, with robustness and effectiveness superior to PID controllers. Zhao et al. [25] used radial basis neural networks to compress unknown system terms and external disturbances into unknown parameters, aiming at the problem of course control and maintenance with unknown environmental interference and model uncertainty. Finally, numerical simulation verified the effectiveness of the algorithm. Le et al. [26] studied the application of artificial neural networks in ship heading control systems. A two-layer multi-layer feedforward neural network heading control system is proposed. The simulation results show that the course control system can maintain the predefined direction under various sea conditions, and the proposed method can be used to develop and apply the design of a real ship automatic driving system. To sum up, the combination of neural networks and fuzzy logic control can effectively resist

the interference of the external environment. It has stability and generalization. This kind of controller meets the requirements of current navigation practice.

ANFIS combines the advantages of artificial neural networks (ANNs) and fuzzy inference systems (FISs). This hybrid control has the advantages of both neural network and fuzzy inference algorithms to achieve better control performance [27]. Compared with the sigmoid PID controller, BELBIC PID controller, and other PID controllers mentioned above, the ANFIS controller can automatically adjust fuzzy rules and parameters through training data, and has strong learning ability without manual intervention. The sigmoid PID controller lacks adaptive learning ability and requires manual parameter adjustment. Although the BELBIC PID controller has certain adaptability, its learning mechanism is relatively complex and depends on the accuracy of the motion model. Therefore, the ANFIS controller can automatically adjust the control strategy by combining fuzzy rules and a neural network to adapt to different sea conditions and ship states. This integration enables the handling of intricate nonlinear relationships, enhancing control accuracy and robustness while maintaining ship course stability in complex maritime environments.

PID controllers require manual adjustment of parameters and cannot control complex nonlinear models. Robust controllers (SMC) are very sensitive to parameter selection, and small changes in parameters can lead to significant changes in controller performance. Therefore, using an ANFIS controller can overcome the shortcomings of the previous two.

In this study, the ANFIS controller based on the MMG model realizes stable ship course control. Rudder angle and propeller speed are used as input parameters to analyze the response performance of the controller. The main contributions can be summarized as follows:

(1) By establishing an MMG model considering the influence of waves, the accuracy of the MMG model is verified by the rotating circle test of the self-propelled model. A large amount of training data comes from a linear control system based on the MMG model, which takes propeller speed and rudder angle as two control inputs and yaw angle speed as the control output. After training, ANFIS takes the difference between the actual course and the expected course, yaw angular speed as input, and rudder angle as output. Course control is executed under both normal and adverse sea conditions. The effectiveness of the proposed ANFIS controller is verified. The MMG model and ANFIS controller can accurately describe the ship's motion characteristics and provide a reliable theoretical basis for the design and verification of the ship's course controller.

(2) By combining the learning ability of a neural network and the reasoning ability of fuzzy logic, a heading controller without manual parameter adjustment is designed. This kind of controller can realize the effective and high-precision control of the desired course and improve the automation level of ship course control.

(3) Simulation tests are carried out under normal sea conditions and bad sea conditions, and the results show that the ANFIS controller is superior to the traditional linear controller in course control performance. In normal sea conditions, the ANFIS controller is able to maintain course with greater accuracy, despite consuming slightly more energy. In harsh sea conditions, the ANFIS controller automatically obtains the best control response through the learning ability of the neural network, showing better robustness. Finally, the influence of propeller speed variation on ship course and rudder angle response is analyzed, which provides theoretical support for ship control in actual sailing.

2. Ship Motion Simulation Model

2.1. Coordinate System

To study the mathematical model of ship motion, it is essential to establish a coordinate system. Two right-handed rectangular coordinate systems are considered, as illustrated in

Figure 1. In the presence of waves in a complex ocean environment, denoted by χ as the wave angle, The *O-XYZ* is the global coordinate system. Point *O* is usually chosen as the position of the ship's center of gravity at the initial moment. In this system, the *OX* axis points due north, *OY* points due east, and *OZ* points toward the center of the earth. The *o-xyz* is the body-fixed coordinate system, with *o* as the midpoint of the line connecting the ship's bow and stern. In this system, *ox* points to the bow along the ship's centerline, and *oy* points to the port side. The heading angle ψ is referenced from the north direction, the rudder angle δ is positive for the right rudder, and *r* is positive in the clockwise direction. In many ship motions and control scenarios, heaving, pitching, and rolling motions are often negligible, simplifying the problem to a plane motion with only 3 degrees of freedom.

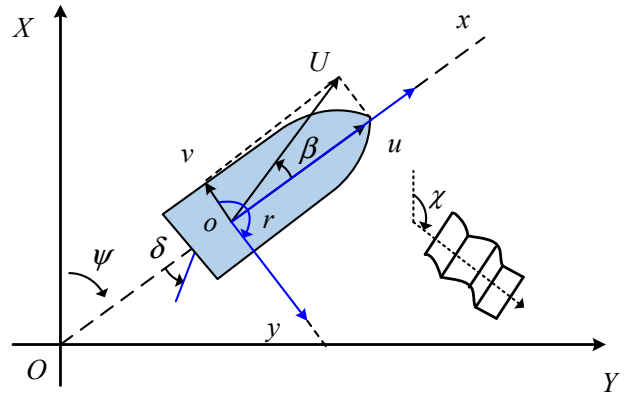


Figure 1. Describes the motion of the ship in the inertial coordinate system and the attached coordinate system.

2.2. 3-DOF MMG Model

The MMG model primarily focuses on decomposing the fluid forces and moments acting on a ship into components related to the bare hull, open water propeller, and open water rudder, as well as their interactions [28]. This decomposition allows for a clearer understanding of the physical forces at play and can be easily supported by experimental data. By establishing a mathematical model of ship motion that considers the interactions between these components, the MMG model addresses issues such as path tracking and heading control. The model simplifies the analysis by only considering the ship's movement with three degrees of freedom on the horizontal plane, omitting rolling, pitching, and heaving motions. Following the separated modeling approach, the study divides the hydrodynamic forces and moments into contributions from the hull, propeller, and rudder. The model expresses the external forces and torques affecting the ship's motion, *X*, *Y*, and *N*, as fluid inertia forces, fluid viscosity forces acting on the hull, propeller thrust, and rudder forces. The basic structure of the MMG model is captured in Equation (1).

$$\begin{cases} m(\dot{u} - vr) = X_I + X_H + X_P + X_R \\ m(\dot{v} + ur) = Y_I + Y_H + Y_P + Y_R \\ I_{zz}\dot{r} = N_I + N_H + N_P + N_R \end{cases} \tag{1}$$

The subscripts *H*, *P*, and *R* denote the low-frequency hydrodynamic forces on the hull, propeller, and rudder, respectively. The subscript *I* denotes the hull fluid inertial force. When a ship changes speed or turns in a fluid, it induces acceleration or deceleration in the surrounding medium, resulting in a reaction force called fluid inertia force. This force, associated with acceleration, hinders the non-inertial motion of the ship in the respective direction.

The fluid inertia force acting on the hull in Equation (1) can be expressed as the following Equation (2).

$$\begin{cases} X_I = -(m_x\dot{u} - m_y vr) \\ Y_I = -(m_y\dot{v} + m_x ur) \\ N_I = -J_{zz}\dot{r} \end{cases} \tag{2}$$

Substituting Equation (2) into Equation (1), the MMG model can be written as follows

$$\begin{cases} (m + m_x)\dot{u} - (m + m_y)vr = X_H + X_P + X_R \\ (m + m_y)\dot{v} + (m + m_x)ur = Y_H + Y_P + Y_R \\ (I_{ZZ} + J_{ZZ})\dot{r} = N_H + N_P + N_R \end{cases} \tag{3}$$

From Equation (3), it is evident that the fluid inertia force results in an increase in the mass and inertia moment of the hull by a specific value. where m is the mass of a ship. m_x and m_y are the added masses along the x and y axes, respectively. I_{zz} and J_{zz} denote inertia moments and the added inertia moments about the Z axis, respectively.

2.2.1. Hydrodynamic Forces Acting on the Hull

Hydrodynamic forces acting on hull can be expressed as follows

$$\begin{cases} X_H = 0.5\rho L^2 V^2 X'_H(v', r') - R(u_0) \\ Y_H = 0.5\rho L^2 V^2 Y'_H(v', r') \\ N_H = 0.5\rho L^3 V^2 N'_H(v', r') \end{cases} \tag{4}$$

where $R(u_0)$ means the ship resistance. X_H, Y_H, and N_H, represent the surge force, sway force, and yaw moment, respectively. The total speed V is expressed as $V = \sqrt{v^2 + u^2}$. L is the length between perpendiculars. The non-dimensional forms of r and v are $r\prime = r(L/u)$ and $v\prime = v/V$.

The hydrodynamic coefficients for dimensionless maneuvering are represented in polynomial form with respect to v' and r'

$$\begin{cases} X'_H(v, r') = X'_{vv}v'^2 + X'_{vr}vr' + X'_{rr}r'^2 \\ Y'_H(v, r') = Y'_v v' + Y'_r r' + Y'_{vvv}v'^3 + Y'_{vvr}v'^2 r' + Y'_{vvv}v'^2 + Y_{rrr}r'^3 \\ N'_H(v, r') = N'_v v' + N'_r r' + N'_{vvv}v'^3 + N'_{vvr}v'^2 r' + N'_{\mathrm{vrr}}v' r'^2 + N_{rrr}r'^3 \end{cases} \tag{5}$$

The non-dimension coefficients $X\prime_{vv}$, $X\prime_{vvv}$, $N\prime_{vvv}$, etc., denote hydrodynamic derivatives with respect to physical variables, and they can be obtained by either the planar motion mechanism test or the circular motion test. The hull force is represented as a third-order polynomial, as depicted in Equation (5). The maneuvering coefficients $X\prime_{vv}$, $Y\prime_{vvv}$, and $N\prime_{vvv}$ utilized in this study were obtained through planar motion mechanism (PMM) experiments [29]. This formula illustrates that the hull force can be approximated by a third-order polynomial [30].

2.2.2. Hydrodynamic Forces on the Propeller

Due to the minimal impact of the lateral force and moment of the propeller, accurately measuring their values poses a challenge. In the MMG model, these forces are typically considered in conjunction with the hydrodynamic force of the steering hull, thus being incorporated into Equation (3) while torque is omitted. As a result, the calculation focuses solely on the longitudinal hydrodynamic force of the propeller, specifically the thrust. The propeller thrust is commonly determined using the following formula.

$$X_p = (1 - t_p)\rho n_p^2 D_p^4 K_T \tag{6}$$

In Equation (6), t_p, n_p, and D_p represent the thrust derating coefficient, propeller speed, and propeller diameter, respectively. The thrust coefficient K_T is a function of the advance speed coefficient and is expressed as a second-order polynomial.

$$K_T(J_p) = j_0 + j_1 J_p + j_2 J_p^2 \tag{7}$$

The coefficients j_0, j_1, and j_2 in Equation (7) can be determined through propeller open water testing, and the advance speed coefficient J_p is expressed as

$$J_p = \frac{u(1-w_p)}{nD} \tag{8}$$

Equation (8) defines w_p as the wake coefficient at the propeller, with its value typically varying during maneuvering motion. This article employs a specific formula to estimate w_p.

$$w_p = w_{p0} \cdot \exp(-8.0\beta_p^2) \tag{9}$$

In Equation (9), w_{p0} represents the wake fraction at the propeller when the ship is sailing straight, and β_p represents the inflow angle at the propeller during maneuvering motion.

$$\beta_p = \beta - x'_p r' = \tan^{-1}(-v/u) - x'_p r' \tag{10}$$

In Equation (10), $\beta = \tan^{-1}(-v/u)$ represents the drift angle, and $x\prime_p$ represents the dimensionless x-coordinate of the propeller.

2.2.3. The Rudder Forces

For ship maneuverability, the calculation of rudder force is of paramount importance. The rudder forces are evaluated as

$$\begin{cases} X_R = -(1-t_R)F_N \sin\delta \\ Y_R = -(1+a_H)F_N \cos\delta \\ N_R = -(x_R + a_H x_H)F_N \cos\delta \end{cases} \tag{11}$$

where F_N is the rudder normal force. t_R, a_H and x_H represent the interaction coefficients between ship hull and rudder. x_R denotes the x coordinate of the center of the rudder.

The rudder normal force F_N is evaluated by

$$F_N = \frac{1}{2}\rho \frac{6.13\Lambda}{\Lambda + 2.25} A_d U_R^2 \sin\alpha_R \tag{12}$$

where ρ is the water density. Λ and A_d are the rudder aspect ratio and the rudder area, respectively. U_R and α_R represent the resultant rudder inflow velocity and the inflow angle, respectively, and they can be estimated as follows

$$\begin{cases} \alpha_R = \delta - \tan^{-1}(v_R/u_R) \\ u_R = u_p \varepsilon \sqrt{1 + 8\kappa K_T/(\pi J_P^2)} \\ u_p = u\left[(1-w_p) + \tau\beta_p^2\right] \\ v_p = \left(\gamma v' + C_{Rr} r' + C_{Rrrr} r'^3 + C_{Rrrv} r'^2 v'\right) U \\ U_R^2 = u_R^2 + v_R^2 \end{cases} \tag{13}$$

where the coefficients ε, κ, τ and γ represent the interaction among the hull, propeller, and rudder. v_R is the inflow velocities of the rudder in the x direction. C_{Rr}, C_{Rrrr} and C_{Rrrv} are experimental constants for expressing v_R accurately [31]. u_R and u_P are the inflow velocities

to the rudder and the propeller, respectively. K_T, $w_{p,}$ and J_p are the propeller thrust, the wake coefficient, and the propeller advanced ratio, respectively.

2.3. Wave Disturbance

Ships navigating the sea are inevitably influenced by waves, and a precise description of the wave disturbances experienced by ships is crucial for accurate analysis in ship maneuvering control research. To predict the wave disturbance affecting a ship, this study employs the modified Pearson–Moscowitz (MPM) spectrum, which is detailed as follows

$$S_{\zeta\zeta}(\omega) = \frac{4\pi^3 H_s^2}{T_z^4} w^{-5} \exp(-\frac{16\pi^3}{T_z^4}\omega^{-4}) \tag{14}$$

where H_s is the significant wave height. T_z is the average zero-crossings period. One 2nd-order linear shape function W_r is utilized to approximate the wave disturbance acting on course. It is expressed as follows

$$W_r = h_r(s) \cdot W(s) \cdot \sin(\psi - \chi) \tag{15}$$

where $W(s)$ is the zero-mean Gaussian white noise and its power spectrum1.0. One 2nd-order wave transfer function $h_r(s)$ is approximately described as

$$h_r(s) = \frac{2\xi_0\omega_0\sigma_r s}{s^2 + 2\xi_0\omega_0 s + {\omega_0}^2} \tag{16}$$

where σ_r denotes the dominated wave strength coefficients of Yaw. ξ_0 and ω_0 are the damping coefficient and the dominating wave frequency, respectively. The ξ_0 is chosen as 0.26 in the present study [32]. Substituting $s = \bar{j}\omega(\bar{j}^2 = -1)$ into Equation (11) yields

$$h_r(\bar{j}\omega) = \frac{2\bar{j}\xi_0\omega_0\sigma_r\omega}{(\omega_0^2 - \omega^2) + 2\bar{j}\xi_0\omega_0\omega} \tag{17}$$

The $P_{yy}(\omega)$ is showed as follows

$$P_{yy}(\omega) = \left|h_r(\bar{j}\omega)\right|^2 P_{\omega\omega}(\omega) = \frac{4(\xi_0\omega_0\sigma_r)^2\omega^2}{\left(\omega_0^2 - \omega^2\right)^2 + 4(\xi_0\omega_0\omega)^2} \tag{18}$$

where $P_{\omega\omega}(\omega)$ is selected as 1.0. P_{yy} reflects the energy distribution of $S_{\xi\xi}(\omega)$ in the actual frequency range. When $\omega = \omega_0$, the maximum value of $P_{yy}(\omega)$ is obtained, which is

$$\max P_{yy}(\omega) = P_{yy}(\omega_0) = \sigma_r^2 \tag{19}$$

when $P_{yy}(\omega)$ obtains the maximum value, use $P_{yy(\omega)}$ to approximate the MPM spectrum. At this time, the expressions of ω_0 and σ_r can be obtained

$$\begin{gathered} (\frac{dS_{\zeta\zeta}(\omega)}{d\omega})_{\omega=\omega_0} = 0 \\ P_{yy}(\omega_0) = S_{\zeta\zeta}(\omega_0) = \sigma_r^2 \end{gathered} \tag{20}$$

According to Formula (20), we can get

$$\begin{gathered} \omega_0 = \sqrt[4]{\frac{4}{5} \times \frac{16\pi^3}{T_z^4}} \\ \sigma_r = H_s \times \sqrt{0.0201 T_z} \end{gathered} \tag{21}$$

when the wave spectrum changes, the expressions of ω_0 and σ_r also need to be rederived according to Equation (20). When the encounter frequency ω replaces the wave frequency ω_0 and is substituted into Equation (17), considering infinite water depth and the influence of the ship's forward speed, the resulting output can be obtained.

$$h_r(s) = \frac{2\xi_0\omega\sigma_r s}{s^2 + 2\xi_0\omega s + \omega^2} \tag{22}$$

In summary, the three-degree-of-freedom MMG model has a high degree of nonlinearity and is suitable for ship course control research. The relationship between this model and the wave force model is shown in Figure 2 below.

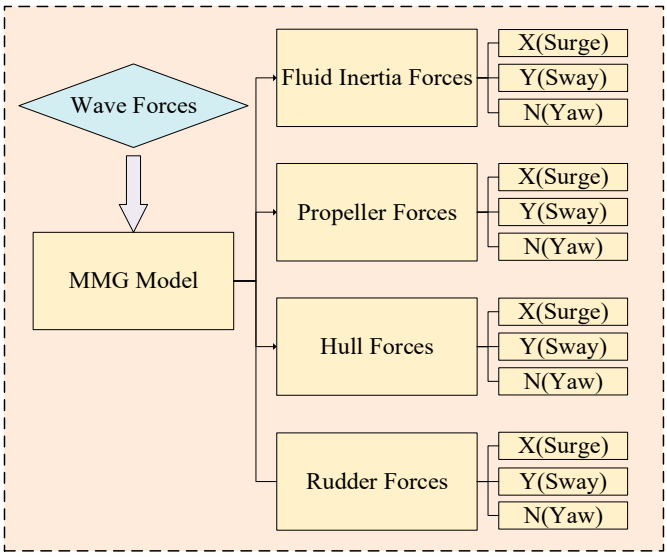


Figure 2. The relationship between this model and the wave force model.

3. Adaptive Neuro-Fuzzy Inference System

The adaptive neuro-fuzzy inference system aims to integrate the fuzzy inference system, which is built on the Takagi–Sugeno model's characteristics and structure, with the learning abilities of neural networks. The Takagi–Sugeno model is a valuable tool for modeling uncertain systems, especially for approximating nonlinear functions and complex dynamic processes.

ANFIS has garnered interest for its innovative approach to system modeling, effectively mapping intricate relationships between input and output data through the integration of learning data and adjustments to membership functions and fuzzy rule parameters. This process involves a neural network-like structure, where the parameters of the fuzzy controller are iteratively optimized based on feedback until the control effect meets a predetermined standard. ANFIS shows promising potential in ship heading control applications.

Figure 3 shows the structure of the ANFIS control system based on the MMG model. The ANFIS controller calculates the rudder angle correction instruction according to the deviation between the set course and the actual course, and the instruction acts on the ship through the actuator to adjust the course. The MMG model simulates the dynamic response of a ship under the action of rudder angle and considers the influence of wave interference on ship motion. System outputs, including swing distance and heading, are displayed graphically to facilitate analysis of the ship's navigational performance. The purpose of the entire system is to keep the ship's course stable by automatically adjusting the rudder angle, even in the case of external disturbances such as waves.

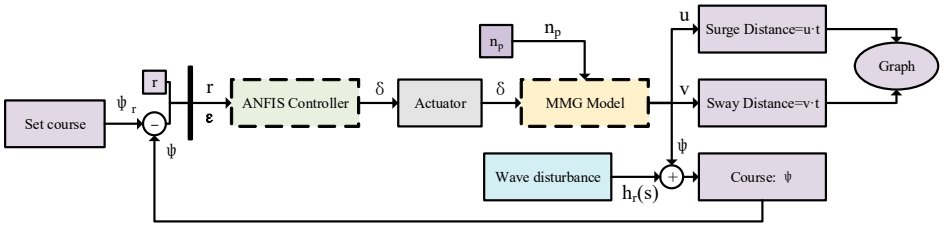


Figure 3. The structure of ANFIS control system based on MMG model.

The training data [*Y*1, *Y*2, *Y*3] were added to the MATLAB working area. When the training period was set to 50 times, the convergence state was finally presented, and the training error was about 0.04°, as shown in Figure 4, indicating that the accuracy of the training process was satisfactory.

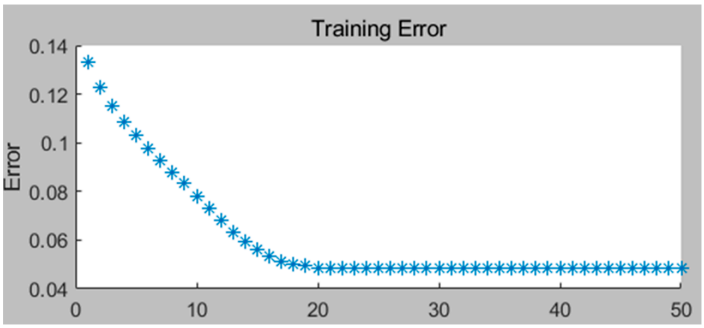


Figure 4. ANFIS training error ("*" represents the training error for each time step).

3.1. ANFIS Ship Heading Controller Structure

The ship's control system operates through a range of sensors, such as gyroscopes, heading sensors, speed sensors, rudder angle sensors, and wave sensors. The sensor feeds some data into the controller and then outputs it.

The ANFIS described in this study is a feedforward fuzzy neural network consisting of 5 layers, as illustrated in Figure 5. It incorporates artificial neural network elements into a fuzzy neural system to create an artificial neural network and applies the learning algorithm of artificial neural networks to derive the inference rules of the fuzzy system.

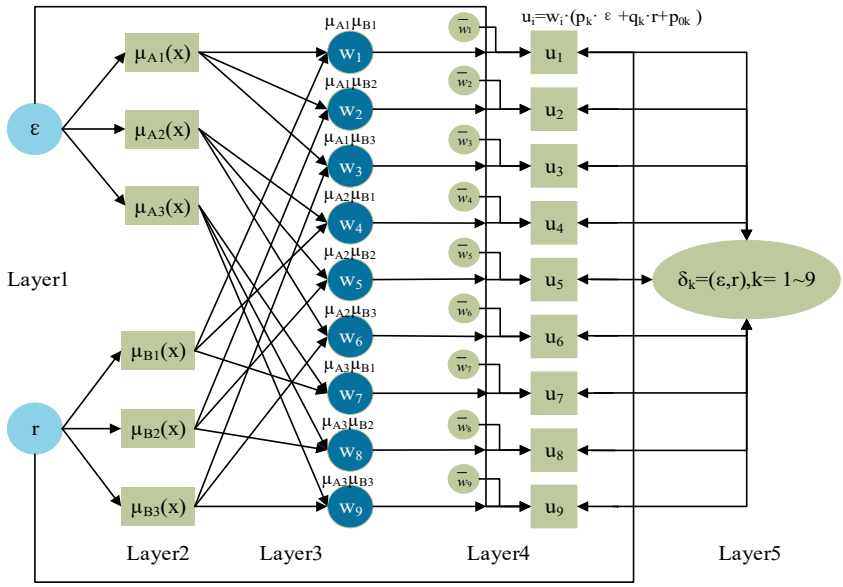


Figure 5. ANFIS with nine rules for two inputs and one output.

Layer1: Input variable layer, the two input variables are the heading error $\varepsilon = \psi_r - \psi$ and the head angular velocity $r = \dot{\psi}$. The first layer simply transmits the input values to the next layer.

Layer2: The input language layer is responsible for fuzzifying the input signal using two input languages ε and r, corresponding to membership functions $\mu_{A1(x)}$, $\mu_{A2(x)}$, $\mu_{A3(x)}$ and $\mu_{B1(x)}$, $\mu_{B2(x)}$, $\mu_{B3(x)}$, respectively. Each square neuron node represents a membership function, and the output of the fuzzification layer is the corresponding membership function. Data clustering technology is utilized to analyze sample data and determine the clustering center of input variables, leading to fuzzy partitioning based on the clustering results.

Layer3: The excitation intensity of each rule is calculated by controlling the rule layer and applying the formula $w_i = \mu_{Ai1}\mu_{Bi2}$, where i ranges from 1 to 3. In this system, 9 Sugeno-type reasoning rules are designed. The rule structure is defined as follows: if ε corresponds to m_{f1} and r also corresponds to m_{f1}, then $\delta = w_k$, where k spans from 1 to 9.

Layer4: The output language layer represents the language value of the controller's output language variable. The front end of the output language layer is the normalized result of all rule strengths and then calculates the output of each rule u_i. Each neural network node corresponds to a specific membership function, which is responsible for delineating the fuzzy boundaries of the language value. It is worth noting that the membership function used adopts the Sugeno model, which is a first-order linear function. This is because of the efficient performance of the Sugeno model. In model construction, if the preconditions are fuzzy, the subsequent results will be clear quantities to ensure the output results' accuracy and reliability.

Layer5: Output variable layer, representing the output variable value of the controller.

3.2. ANFIS Ship Heading Control Optimization Algorithm

In this study, the backpropagation learning algorithm was integrated with the least square method to optimize control parameters using the time backpropagation algorithm, resulting in a hybrid learning algorithm for ANFIS.

The network adjusts its internal parameters by comparing the output with the expected trajectory in each period and fine-tunes itself through error feedback to learn and approximate the desired model behavior. Jang introduced an adaptive neuro-fuzzy inference system by integrating time-backward propagation (TBP), enhancing the traditional backward propagation (BP) learning algorithm. By training the neural network with the TBP mechanism, the controlled system's output can be more effectively guided to accurately track the desired path, leading to a significant enhancement in control system performance. The learning process of the ship heading ANFIS control system using the TBP learning algorithm is illustrated as a closed-loop dynamic simulation behavior in Figure 6. The optimization criterion is to minimize the control performance metric, which is usually expressed as the error between the actual heading and the desired heading.

In Figure 6, Δ represents the time shift factor, $\psi_r(k)$ denotes the heading command, the desired trajectory is formed based on the set heading $\psi_r(j)$, and all $\psi(j)$ is stored to create the actual motion trajectory. The expression of the closed-loop control performance index is an optimization function, as shown in Equation (23). The consequent parameters $\{p_{Ak}, q_{Bk}, p_{0k}\}$ of the Sugeno-type fuzzy rule in ANFIS are determined through the learning law provided by the BP algorithm, as shown in Equation (24).

$$E = \sum_{k=0}^{n} \delta^k (r - \overline{\psi})^2 \tag{23}$$

$$\Delta a_i = -\eta \frac{\partial E}{\partial a_i} = -\eta \sum_{k=1}^{n} \frac{\partial E(j)}{\partial a_i} \tag{24}$$

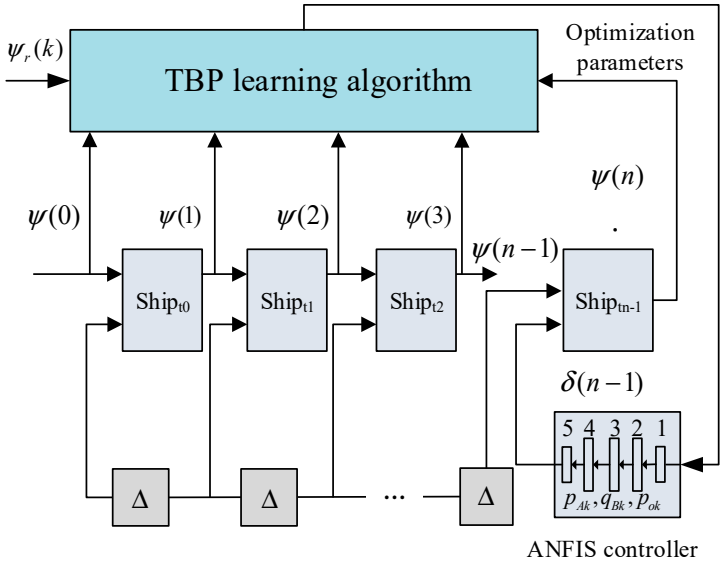


Figure 6. TBP learning process of ship heading ANFIS controller.

Utilizing Equation (24) of the TBP algorithm to optimize the parameter ai, the ANFIS controller can be updated with these parameters and subsequently applied in the next control cycle.

ANFIS's TBP parameter optimization algorithm consists of two main processes: forward calculation and reverse calculation. The forward calculation process addresses the storage and accumulation of data needed for learning through direct calculations, while the reverse calculation process utilizes the TBP algorithm to adjust parameters.

(1) Forward calculation of ANFIS

Layer1: The first layer determines that the two inputs are, respectively, the deviation ε between the ship's current course and the expected course and the heading angular speed r.

$$\varepsilon = \psi_r - \psi; r = \overline{\psi} \tag{25}$$

Layer2: The generalized bell-shaped membership function is determined by the parameters a, b, and c in Formula (26), with a and b typically being positive values. The parameter c is utilized to specify the center of the curve.

$$\mu_{Ai/Bi}(x, a, b, c) = \frac{1}{1 + \left| \frac{x - c}{a} \right|^{2b}}; i = 1, 2, 3 \tag{26}$$

Layer3: Calculate the excitation intensity of each rule, as depicted in Equation (27). Subsequently, normalize each excitation intensity to obtain Equation (28).

$$w_k = \mu_{Ai_1} \mu_{Bi_2}; i_1, i_2 \in \{1, 2, 3\}; k = 1, 2, \cdots, 9 \tag{27}$$

$$\overline{w}_k = \frac{w_k}{\sum_{k=1}^{9} w_k} \tag{28}$$

Layer4: The fourth layer is the output of fuzzy rules. The output of each rule is a linear combination of input variables.

$$\overline{w_k}u_k = \overline{w_k}(p_{Ak}\varepsilon_k + p_{Bk}r_k + p_{0k}) \tag{29}$$

Layer5: The output is the command rudder angle given by the ANFIS autopilot, which is affected by the consequent parameters $\{p_i, q_i, p_{0k}\}$.

$$\delta_k = \sum_{k=1}^{9} \overline{w_k}u_k \tag{30}$$

(2) Reverse calculation of ANFIS

During a sampling period, the parameters in Equation (24) are represented with simplified symbols: $E(j) = E_j$, $\varepsilon(j) = \varepsilon_j$, $\psi(j) = r_j$, $\delta r(j) = \delta rj$, $w_k = w^k$, $\overline{w_k} = \overline{w^k}$, $\overline{w_A}(k) = \overline{w_A^k}$, $\overline{w_B}(k) = \overline{w_B^k}$,$u_k = u^k$, $u_k(j) = u^j k$.

$$\frac{\partial E}{\partial a_k} = 2\sum_{j=1}^{n} \varepsilon_j t_j \frac{\partial \varepsilon_j}{\partial a_k} \tag{31}$$

$$\frac{\partial \varepsilon_j}{\partial a_k} = \frac{\partial \varepsilon_j}{\partial \psi_j} \cdot \frac{\partial \psi_j}{\partial \delta_j} \cdot \frac{\partial \delta_j}{\partial \delta_{rj}} \cdot \frac{\partial \delta_{rj}}{\partial a_k} = \frac{\partial \psi_j}{\partial \delta_j} \cdot \frac{\partial \delta_j}{\partial \delta_{rj}} \cdot \frac{\partial \delta_{rj}}{\partial a_k} \tag{32}$$

From Equation (33), Equation (34) can be derived.

$$\delta_{rj} = \sum \overline{w_j^k} u_j^k \tag{33}$$

$$\frac{\partial \delta_{rj}}{\partial a_k} = \begin{cases} \overline{w_j^k}\varepsilon_j, a_k = p_{Ak} \\ \overline{w_j^k} r_j, a_k = p_{Bk} \\ \overline{w_j^k}, a_k = p_{0k} \end{cases} \tag{34}$$

By comprehensively applying Equations (23) to (34), we can solve the problem of updating the controller consequent parameters $\{p_{Ak}, q_{Bk}, p_{0k}\}$.

To sum up, the ANFIS structure shown in Figure 5 needs to be learned based on the TBP learning algorithm. The control object is the MMG model, which constitutes the control system shown in Figure 2.

4. Model Validation

4.1. Free Self-Propelled Model Test

In general, the more exact a control plant is established, the more accurate control performances can be evaluated. In the present study, the control plant is obtained from the free-running model tests, which were conducted at the ocean engineering wave basin in Shanghai Jiao Tong University. The dimension of the basin is 50 m × 30 m. A high-fidelity MMG model mentioned in Section 2.2 is adopted for the S175 ship, whose main particulars are described in Table 1. The model test and numerical simulations are carried out based on the ship model with a scale ratio of 1:57.686.

According to the turn test defined in Figure 7, the tactical diameter and forward distance need to be determined. The International Maritime Organization (IMO) requires a tactical diameter of less than 5.0 L and a forward distance of less than 4.5 L.

Table 1. Principal particulars of ship models.

	Items	Units	Full Scale	Model
Hull	Length between perpendiculars, L	m	175.0	3.0337
	Beam, B	m	25.4	0.4403
	Draft, D	m	9.5	0.1647
	Displacement, ∇	m_3	24,742	0.127
	Block coefficient, C_B	/	0.57	0.57
	Radius of gyration in roll, k_{xx}	/	0.33 B	0.33 B
	Radius of gyration in pitch, k_{yy}	/	0.25 L	0.25 L
	Radius of gyration in yaw, k_{zz}	/	0.269 L	0.269 L
Propeller	Diameter, D_p	m	6.5064	0.1128
	Pitch ratio	/	0.915	0.915
	Number of blades	/	5	5
Rudder	Area, A_d	m^2	32.46	0.0098
	Height, H	m	7.7	0.1335
	Aspect ratio, Λ	/	1.8268	1.8268

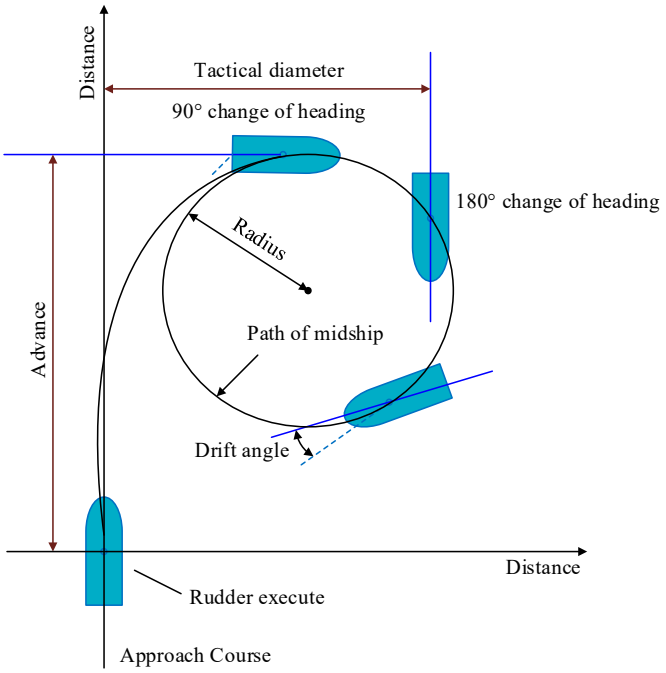


Figure 7. Notations and criteria in turning test.

4.2. Numerical Simulation of Rotary Motion in Still Water

Zou Z.J.'s team at Shanghai Jiao Tong University conducted a self-propelled model rotation test in still water to obtain reliable data. The interference coefficients and hydrodynamic derivatives for the ship-propeller-rudder system were computed and are presented in detail in Table 2. The shape factor k_f and residual resistance coefficient C_r for the hull were estimated using empirical formulas provided. Additional coefficients can be found in the PMM test data of Yasukawa [33].

The rotation trajectory of the S175 container ship model in still water is illustrated in Figure 8. The dimensions of the ship model, initial velocity, propeller speed, and rudder speed were all kept constant throughout the test. Upon comparing the numerical simulation findings with the experimental rotation trajectory in still water, a high level of agreement was observed.

Table 2. Hydrodynamic derivative and interference coefficient in S175 maneuvering motion model.

	Symbol	Value	Symbol	Value	Symbol	Value
Hull	m'_x	0.000238	Y'_v	−0.0116	N'_v	−0.00385
	m'_y	0.007049	Y'_r	0.00242	N'_r	−0.00222
	J'_{xx}	0.0000034	Y'_{vvv}	−0.109	N'_{vvv}	0.001492
	J'_{zz}	0.000419	Y'_{vvr}	0.0214	N'_{vvr}	−0.0424
	X'_{vv}	−0.00386	Y'_{vrr}	−0.0405	N'_{vrr}	0.00156
	X'_{vr}	−0.00311	Y'_{rrr}	0.00177	N'_{rrr}	−0.00229
	X'_{rr}	0.0002	z_H/D	0.5	N_{10}	0.0082
	C_r	0.001	kf	1.04		
Propeller	t_P	0.175	1-wp0	0.816	x_P	−0.47
	j_0	0.5179	j_1	−0.1179	j_2	−0.3618
Rudder	t_R	0.29	x'_H	−0.48	x'_R	−0.5
	a_H	0.237	ε	0.921	γ	0.088 ($v' < 0$)
	K	0.631	z_H/D	0.7		0.193 ($v' \geq 0$)
	C_{Rr}	−0.156	C_{Rrr}	−0.275	C_{Rrvv}	1.96

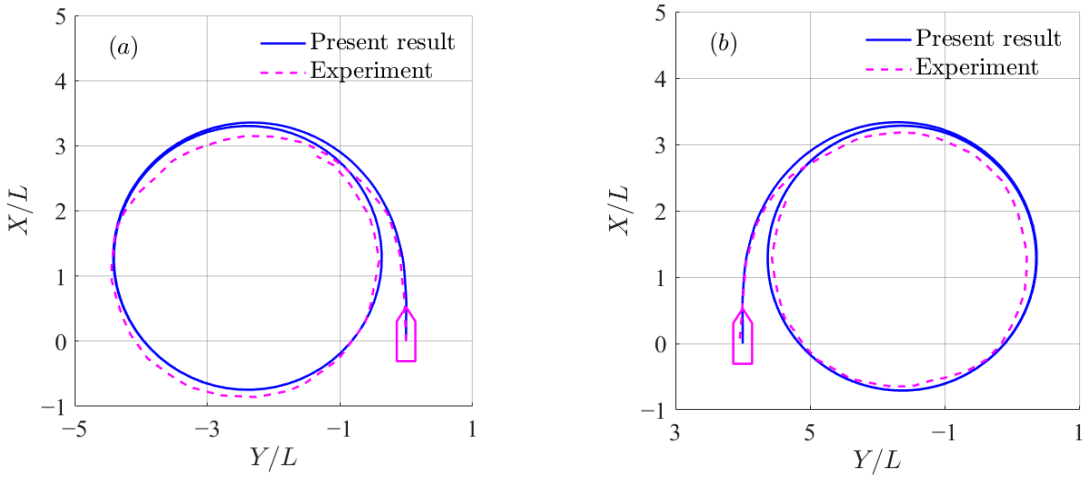


Figure 8. Turning tests in clam water at $F_n = 0.15$: (**a**) port turning ($\delta = -35°$); (**b**) starboard turning ($\delta = 35°$).

Table 3 presents a comparison of the results for rotation diameter, tactical diameter, advance distance, and horizontal distance between numerical simulation and experiment. The relative error E_r is calculated using Equation (35):

$$E_r = \frac{|V_n - V_t|}{V_t} \times 100\% \tag{35}$$

where V_n and V_t denote the values of numerical results and the test results, respectively.

Table 3. Comparison of numerical results and test trajectories.

Parameter Name	Numerical	Test	Relative Error
Tactical diameter ($\delta = -35°$)	4.5 L	4.4 L	2.27%
Tactical diameter ($\delta = 35°$)	4.5 L	4.2 L	7.14%
Advance ($\delta = -35°$)	3.4 L	3.2 L	6.25%
Advance ($\delta = 35°$)	3.4 L	3.1 L	9.68%

The errors of tactical diameter and the advance are about 2.27% and 6.25%, respectively. In addition, the numerical results of the tactical diameter and the advance are 4.5 L and

3.4 L, and they are less than the requirements of 5 L and 4.5 L, respectively. It shows that the MMG model is effective to describe the maneuverability of S175. The results indicate that the MMG model utilized in this study is effective, with satisfactory calculation accuracy. The maneuverability of the S175 container ship is specifically applied in practical navigation scenarios.

5. Results

5.1. Performance Analysis Metrics

The ship uses a controller to control the heading needed to continue sailing through the waves. For further quantitative analysis, the two criteria A_ψ and I_δ evaluate the control performance as follows:

$$\begin{aligned} A_\psi &= \frac{1}{t_\infty - t_0}\int_{t_0}^{t_\infty} |S_\psi - T_\psi| dt \\ I_\delta &= \frac{1}{t_\infty - t_0}\int_{t_0}^{t_\infty} |U_\delta| dt \end{aligned} \tag{36}$$

where S_ψ denotes the desired heading; T_ψ is the actual heading; U_δ is the input rudder; A_ψ represents the mean absolute error of course keeping to measure the response performances of course keeping; I_δ is the mean absolute input of rudder to evaluate energy consumption of rudder engine.

5.2. Simulation of Navigation Trajectory in the Still Sea

The ANFIS controller is utilized to model the ship's sailing trajectory during a simulation lasting 860 s. The ship is traveling north with a speed of F_n = 0.15, while the propeller speed is limited to n_p = 20rps. The wave disturbance caused by Beaufort No. 6 wind is incorporated to introduce white noise with a power of 0.001. In the simulation, λ_ψ = 100 controller is taken as an example to illustrate the control performances. Various desired heading values of 40°, 60°, 90°, 270°, 300°, and 320° are input into the controller. The navigation trajectory is depicted in Figure 9. The outcomes reveal that under normal sea conditions, the actual heading of the navigation trajectory aligns closely with the expected heading, indicating a successful control performance.

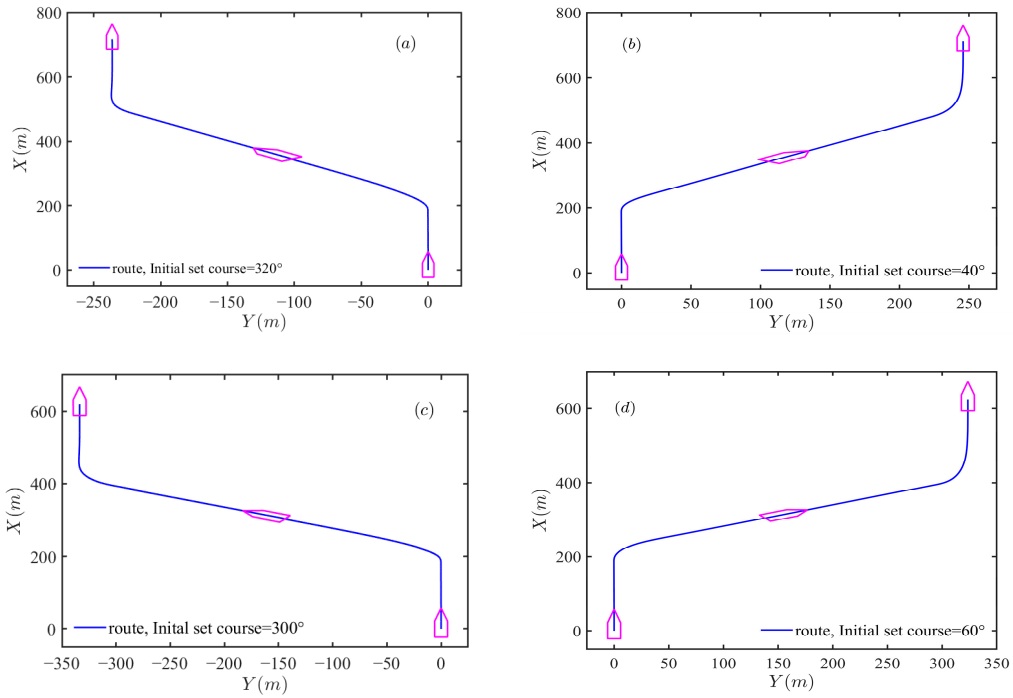


Figure 9. *Cont.*

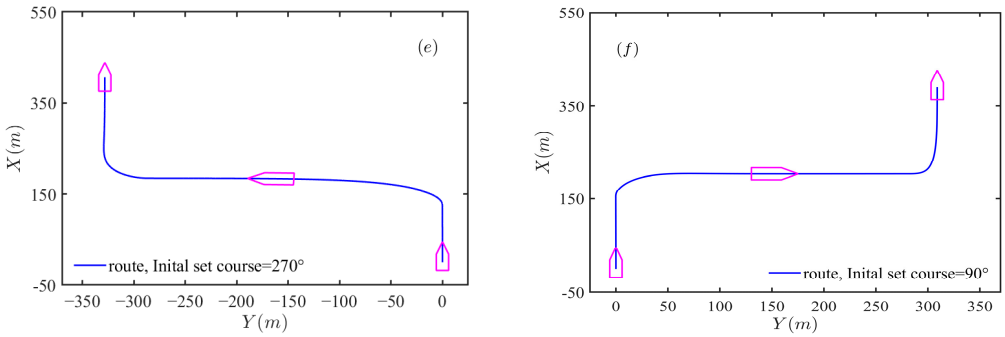


Figure 9. Navigation trajectories of different setting course in clam water conditions: (**a**) 320°; (**b**) 40°; (**c**) 300°; (**d**) 60°; (**e**) 270°; (**f**) 90°.

5.3. Course and Roll Stabilization Performances in the Still Sea

The parameters of the linear controller for generating training data are selected from the literature [34]. The performance parameters of the linear controller can be adjusted to λ_ψ to quantitatively meet different control requirements. The performance parameters can reflect the response characteristics and stability of the controller.

As depicted in Figure 10, the ship initially departs from the due north direction (0°) under normal sea conditions. At 200 s into the simulation, the ship begins to turn and eventually reaches the desired heading, maintaining it thereafter. By 600 s, the ship gradually returns to its initial heading. The simulation can be divided into different stages: 0–200 s for the step duration, 200–400 s for significant heading changes, 400–600 s for heading maintenance, 600–900 s for heading recovery, and 900–1000 s for heading maintenance. Setting the desired headings at 40°, 60°, 90°, 270°, 300°, and 320° initially, both controllers effectively manage the heading throughout the simulation.

As depicted in Figure 11, the simulation experiment enforces a limitation on the ship's rudder speed to a range of $[-5°/s, 5°/s]$, with the rudder angle saturation limit set at $\delta \in [-35°, 35°]$. When there is a deviation in the desired heading, both the controller and linear controller in ANFIS exhibit similar changes in the rudder angle. The simulation results confirm the precision of the training data and demonstrate the effective control performance of both controllers.

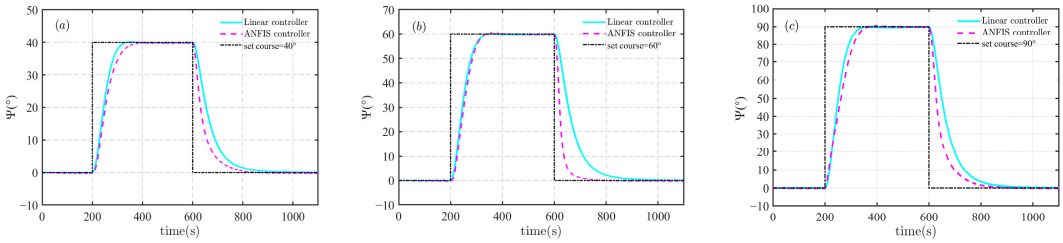


Figure 10. The effect of linear controller and ANFIS controller on ship heading control: (**a**) set course = 40°; (**b**) set course = 60°; (**c**) set course = 90°.

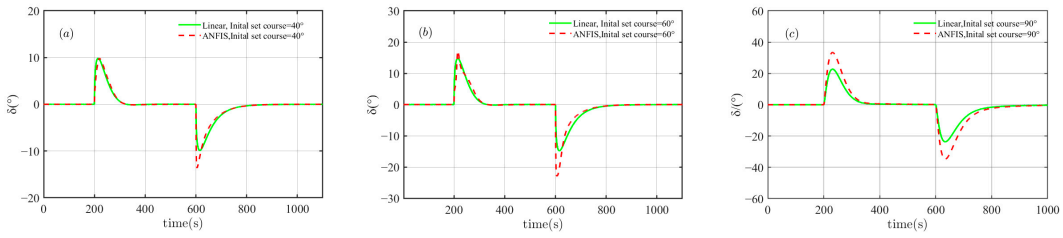


Figure 11. Linear controller and ANFIS controller control ship's rudder angle: (**a**) set course = 40°; (**b**) set course = 60°; (**c**) set course = 90°.

Based on the control effects illustrated in Figures 10 and 11, and in conjunction with Equation (36), the values of A_ψ and I_δ were calculated with λ_ψ set to 100. Tables 4 and 5 present a comparative analysis of the performance between linear controllers and ANFIS controllers during starboard turn operations at initial moments, with expected courses of 40°, 60°, and 90°. For the linear controller, the A_ψ values are 3.02°, 4.62°, and 6.96°, while the corresponding I_δ values are 0.51°, 0.73°, and 1.09°. In contrast, for the ANFIS controller, the A_ψ values are 3.00°, 4.32°, and 5.94°, and the I_δ values are 1.01°, 2.15°, and 2.99°, respectively. When the ship needs to recover its initial course and perform a left turn, the A_ψ values for the linear controller are 4.15°, 6.31°, and 9.16°, and the I_δ values are 0.67°, 0.98°, and 1.47°, respectively. For the ANFIS controller, the A_ψ values are 4.02°, 5.98°, and 7.54°, and the I_δ values are 1.59°, 2.64°, and 3.61°, respectively. The results indicate that both controllers exhibit increasing A_ψ and I_δ values as the expected course increases. While the ANFIS controller demonstrates more stable heading control (smaller A_ψ), this comes at the expense of higher energy consumption (larger I_δ).

Table 4. The analysis of control performance (right rudder).

Symbol	$A_\psi(\psi = 40°)$	$A_\psi(\psi = 60°)$	$A_\psi(\psi = 90°)$	$I_\delta(\psi = 40°)$	$I_\delta(\psi = 60°)$	$I_\delta(\psi = 90°)$
Linear	3.02°	4.62°	6.96°	0.51°	0.73°	1.09°
ANFIS	3.00°	4.32°	5.94°	1.01°	2.15°	2.99°

Table 5. The analysis of control performance (left rudder).

Symbol	$A_\psi(\psi = 40°)$	$A_\psi(\psi = 60°)$	$A_\psi(\psi = 90°)$	$I_\delta(\psi = 40°)$	$I_\delta(\psi = 60°)$	$I_\delta(\psi = 90°)$
Linear	4.15°	6.31°	9.16°	0.67°	0.98°	1.47°
ANFIS	4.02°	5.98°	7.54°	1.59°	2.64°	2.99°/3.61°

As illustrated in Figure 12 and Table 6, when the expected heading is set to 40°, 60°, and 90°, the maximum response rudder angle differences between the ANFIS controller and the linear controller are 0°, 3°, and 11°, respectively. For expected headings of 270°, 300°, and 320°, these differences increase to 3°, 8°, and 29°, respectively. These findings indicate that the maximum response rudder angle of the ANFIS controller exceeds that of the linear controller, with the disparity becoming more pronounced as the expected heading increases. Consequently, the ANFIS controller imposes a higher load on the steering gear. Additionally, while the response times for both controllers are comparable at expected headings of 40°, 60°, and 90°, the ANFIS controller demonstrates significantly faster response times—approximately 28.57%, 43.75%, and 37.78% quicker—at expected headings of 270°, 300°, and 320°, respectively. This evidence underscores the superior response speed of the ANFIS controller compared to the linear controller. In summary, the larger rudder angle responses suggest that the ANFIS controller can more rapidly adjust the ship's control status under typical sea conditions, thereby enhancing the overall dynamic performance of the system.

Table 6. Comparison of the maximum rudder angle and response time of the ship turning.

Symbol	$\psi = 40°$	$\psi = 60°$	$\psi = 90°$	$\psi = 270°$	$\psi = 300°$	$\psi = 320°$
Linear (δ/t)	10°/130 s	14°/145 s	22°/170 s	−10°/350 s	−14°/400 s	−22°/450 s
ANFIS (δ/t)	10°/135 s	17°/135 s	33°/170 s	−13°/250 s	−22°/225 s	−51°/280 s

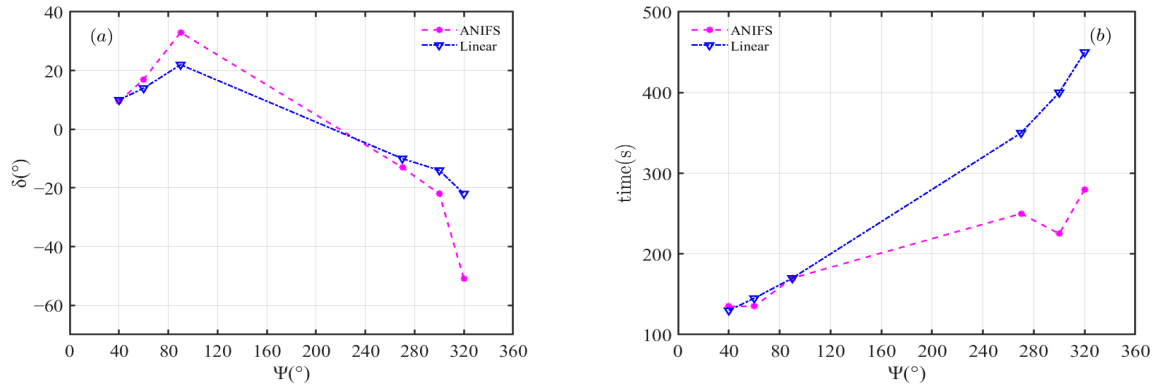


Figure 12. Comparison of the maximum rudder angle and response time of the ship when turning: (**a**) the maximum rudder angle; (**b**) response time.

5.4. Course and Roll Stabilization Performances in the Heavy Sea

According to Figure 13 and Table 7, it can be seen that under bad sea conditions, when the expected heading is 40° and λ_ψ = 100, the response time of the linear controller and ANFIS controller is 100 s and 180 s, respectively, and the response time is reduced by about 33.3%. The A_ψ is 5.24° and 5.85°, and the I_δ is 1.84° and 1.54°, respectively. When the left rudder operation is performed, A_ψ is 7.05° and 6.96°, and I_δ is 1.96° and 1.71°, respectively. The results show that the response time of ANFIS is longer than that of the linear controller, but its I_δ index is smaller. The course stability of the two controllers is basically the same regardless of whether the rudder is turned right or left. It can be concluded that the response time of ANFIS is affected in bad sea conditions, but the stability of ANFIS is better than that of the linear controller during the whole course-keeping phase, and it has better energy-saving characteristics.

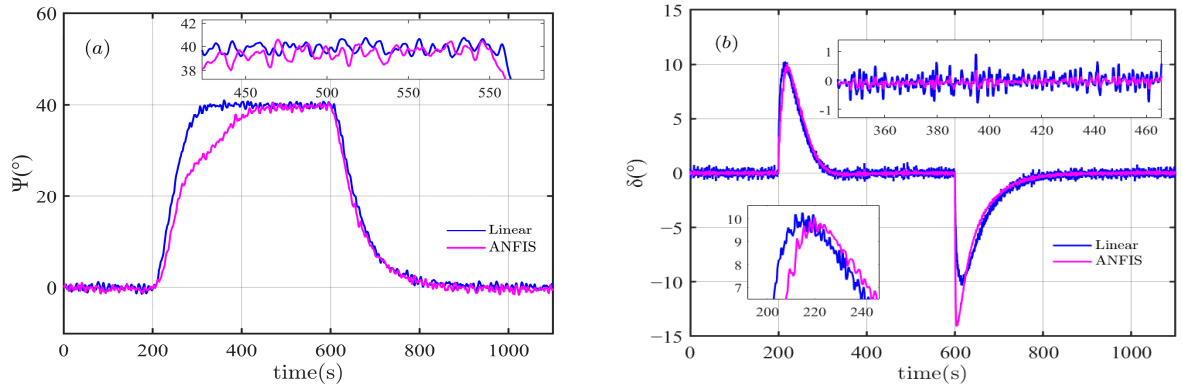


Figure 13. Comparison of steering stability between ANFIS controller and linear controller in the heavy sea: (**a**) course control; (**b**) rudder angle.

Table 7. The analysis of control performance (ψ = 40°).

Symbol	Response Time	$A_\psi(\psi = 40°$, Right Rudder)	$A_\psi(\psi = 40°$, Left Rudder)	$I_\delta(\psi = 40°$, Right Rudder)	$I_\delta(\psi = 40°$, Left Rudder)
Linear	100s	5.24°	7.05°	1.84°	1.96°
ANFIS	180s	5.85°	6.96°	1.54°	1.71°

Figure 14 and Table 8 show small amplitude course control and rudder angle performance (ψ = 60°). It is worth mentioning that course performance is determined by 100–400 s of course change and 400–1000 s of course hold, respectively. As shown in Figure 14a and Table 8, the A_ψ using the λ_ψ = 60, λ_ψ = 90, and λ_ψ = 120 controllers are 2.57°, 3.19°, and

4.14°, respectively, increasing by 24.12% and 29.78%. The controller (λ_ψ = 60) has the fastest response time but has a slight overshoot. The controller (λ_ψ = 120) has the longest response time. The A_ψ of the ANFIS controller is 2.86°, which is only 11.28% higher than that of the linear controller with the best directional stability (λ_ψ = 60), has satisfactory stability and safety, and does not produce an overshoot phenomenon. Figure 14b and Table 8 show that the controller (λ_ψ = 60) has a larger control input (maximum rudder angle) than the other controllers, but its I_δ of 0.79° is the smallest among the three linear controllers with different parameters, due to its fast response speed. The I_δ of the ANFIS controller is 1.12°, which not only has a good energy-saving effect but also has no overshoot.

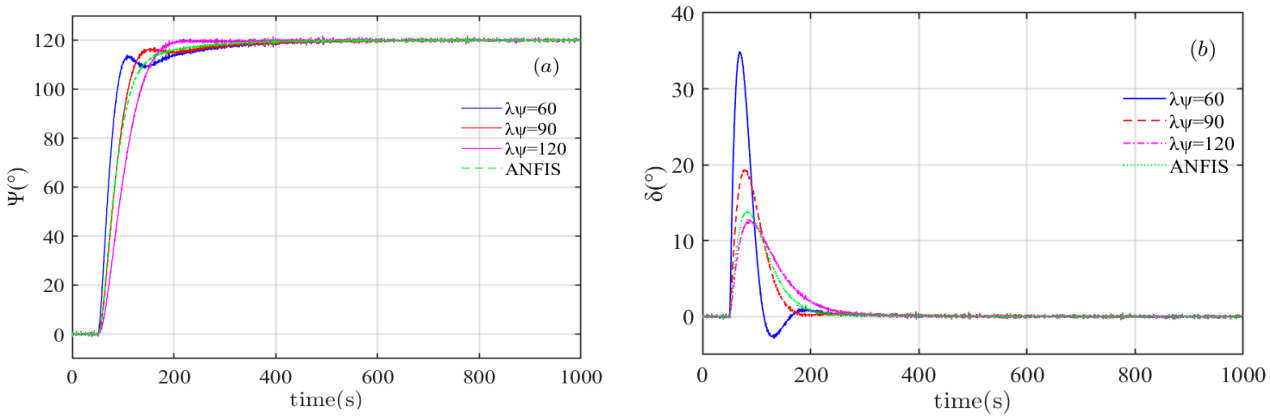


Figure 14. Comparison of course control and rudder angle in the heavy sea between ANFIS controller and linear controller (ψ = 60°): (**a**) course control; (**b**) rudder angle.

Table 8. The analysis of control and rudder performance in the heavy sea between ANFIS controller and linear controller (ψ = 60°/120°).

Symbol	A_ψ ψ = 60°/ψ = 120°	$A_\psi(\lambda_\psi$ = 60) ψ = 60°/ψ = 120°	$A_\psi(\lambda_\psi$ = 90) ψ = 60°/ψ = 120°	$A_\psi(\lambda_\psi$ = 120) ψ = 60°/ψ = 120°	I_δ ψ = 60°/ψ = 120°	$I_\delta(\lambda_\psi$ = 60) ψ = 60°/ψ = 120°	$I_\delta(\lambda_\psi$ = 90) ψ = 60°/ψ = 120°	$I_\delta(\lambda_\psi$ = 120) ψ = 60°/ψ = 120°
Linear	/	2.57°/5.51°	3.19°/7.01°	4.14°/8.52°	/	0.79°/1.76°	1.48°/1.52°	1.46°/1.50°
ANFIS	2.86°/6.28°	/	/	/	1.12°/1.46°	/	/	/

Figure 15 and Table 8 show large course control and rudder angle performance (ψ = 120°). Figure 15a and Table 8 show that the A_ψ using the λ_ψ = 60, λ_ψ = 90, and λ_ψ= 120 controllers are 5.51°, 7.01°, and 8.52°, respectively. They increased by 27.22 percent and 21.54 percent, respectively. The A_ψ of the ANFIS controller is 6.28°, which is second only to the λ_ψ = 60 controller and 13.97% higher. It has satisfactory stability and security. As shown in Figure 15b and Table 8, the I_δ of the linear controller decreases as λ_ψ increases. Notably, the I_δ of the ANIFS controller is measured at 1.46°, which is lower than the minimum value of λ_ψ = 120 for the linear controller. This indicates a superior energy-saving effect achieved by the ANIFS controller.

A linear controller and an adaptive neural fuzzy inference system (ANFIS) controller are designed based on the validated MMG model. A propeller speed limit ($0 \leq n_P \leq 40$ rps) was added to the simulation. The linear controller can quantitatively adjust the performance parameters λ_ψ to meet different control requirements. Any controller must be compared to a typical controller to account for its performance. In this paper, a linear controller is established with λ_ψ = 60, λ_ψ = 90, and λ_ψ = 120 as examples. The ANFIS controller operates on the basis of the training data and performs a small heading control (ψ = 60°) and a large heading control (ψ = 120°), respectively. For fair comparison, simulation parameters, wave interference (bad sea conditions), and propeller speed (n_P = 20 rps) were the same for all three controllers.

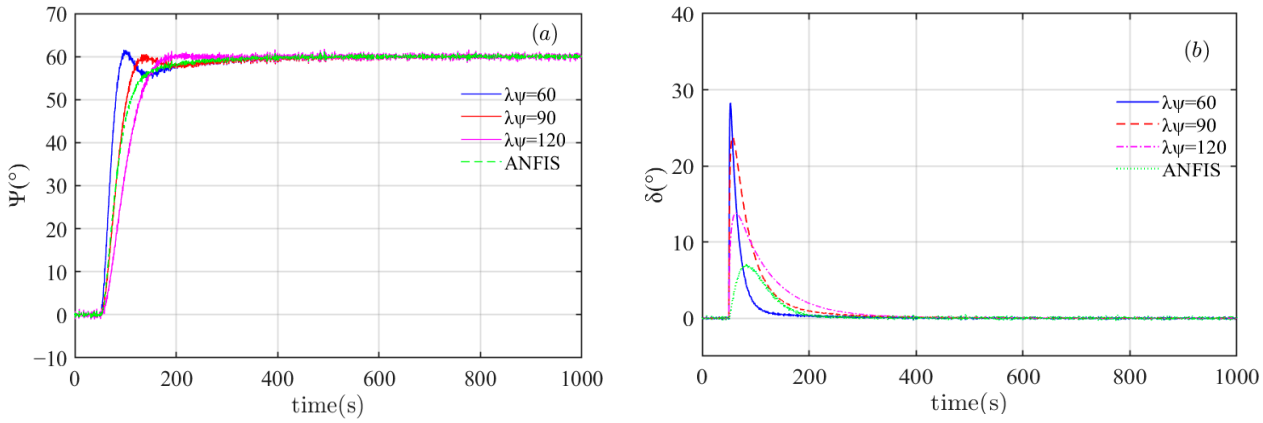


Figure 15. Comparison of course control and rudder angle in the heavy sea between ANFIS controller and linear controller (ψ = 120°): (**a**) course control; (**b**) rudder angle.

The conclusion is that the increase in the parameter λ_ψ improves the response speed of the linear controller, enhances the energy-saving effect of the controller, and increases the volatility of the controller. This makes it impossible to get the best of both worlds by manually adjusting parameters. Although the smallest λ_ψ controller has strong stability and a good energy-saving effect in the course-keeping stage, it will cause overshoot in the response stage, which will cause damage to the steering gear and is not conducive to the safe navigation of the ship. Adaptive neural fuzzy inference system (ANFIS) can be based on the coupling of a neural network and an adaptive fuzzy controller, without manual adjustment, and can automatically adjust the performance parameters to achieve the control effect that the linear controller cannot achieve, so as to adapt to the interference of the external environment. The overshoot phenomenon is overcome, and the stability and energy saving of heading control are effectively enhanced, which shows that the neural network has strong generalization ability and the fuzzy controller is robust.

Figure 16a shows that when the controller performance parameter λ_ψ (λ_ψ = 100) and environmental disturbance remain unchanged, the increase in propeller speed will accelerate the system response, but there will be slight overshooting. Figure 16b shows that the maximum rudder angle remains basically constant at different speeds, while the system oscillation increases slightly with increasing speed. Table 9 lists the A_ψ and I_δ values of the linear controller and ANFIS controller at different propeller speeds. For the linear controller, when the propeller speed is n_P = 10 rps, n_P = 20 rps, and n_P = 30 rps, the A_ψ value is 5.24°, 2.79° and 1.99°, respectively, with a decrease of about 62.02%. For ANFIS controllers, the A_ψ values at these speeds are 5.31°, 2.92°, and 1.98°, respectively, representing a reduction of about 62.71%. The results show that the performance of both controllers is improved with the increase in propeller speed. Linear controller in n_P = 10 rps, n_P = 20 rps, and n_P = 30 rps when I in the delta value is 3.04°, 1.71°, and 1.31°, respectively. Similarly, at these speeds, the I_δ values of the ANFIS controller are 3.03°, 1.71°, and 1.30°, respectively. The results show that the two controllers can achieve a comparable energy-saving effect, and the best energy efficiency is observed at n_P = 30 rps.

Table 9. The analysis of control and rudder performance in the heavy sea between ANFIS controller and linear controller (ψ = 40°).

Symbol	$A_\psi(n_P$ = 10 rps)	$A_\psi(n_P$ = 20 rps)	$A_\psi(n_P$ = 30 rps)	$I_\delta(n_P$ = 10 rps)	$I_\delta(n_P$ = 20 rps)	$I_\delta(n_P$ = 30 rps)
Linear	5.24°	2.79°	1.99°	3.04°	1.71°	1.31°
ANFIS	5.31°	2.92°	1.98°	3.03°	1.71°	1.30°

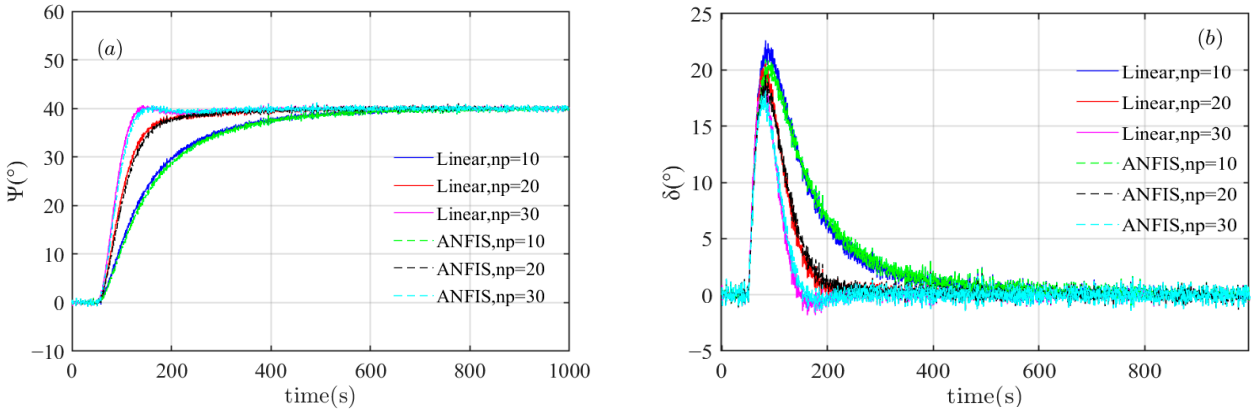


Figure 16. Comparison of course control and rudder angle in the heavy sea between ANFIS controller and linear controller (λ_ψ = 100): (**a**) course control; (**b**) rudder angle.

The conclusion is that appropriate np is necessary when environmental disturbances and other performance parameters are constant because excessive overshoot and errors should be avoided when ships are performing rescue missions or sailing in limited waters. Under the influence of different speeds, the response characteristics of the ANFIS controller are almost the same as those of the linear controller, which shows that the ANFIS controller using the combination of a neural network and fuzzy control has good practicability and generalization.

6. Conclusions

The three-degree-of-freedom MMG model was adopted and verified by the data of the S175 free model turning circle. In order to achieve efficient and stable course control performance, the ANFIS controller is designed by combining the backpropagation algorithm and the least square method. The MMG model is controlled by the linear control method and the ANFIS method, respectively, in normal sea states and bad sea states. Heading error, output rudder angle, and yaw angular speed in the linear controller are the training data sources of ANFIS. ANFIS trains and controls the MMG model through the powerful learning ability of the neural network, simulating and analyzing the performance of the two controllers.

In normal sea conditions, for course control performance, ANFIS can output the correct course trajectory according to the input rudder angle of the MMG model, and A_ψ is lower than the linear controller, which has stronger course stability performance and faster response speed. The maximum output rudder angle of the ANFIS controller is greater than that of the linear controller, and the energy-saving effect is slightly weaker than that of the linear controller.

In harsh sea conditions, the ANFIS controller achieved an I delta improvement of nearly 16% and 13%, respectively, over the linear controller, both on the left and right rudder, while maintaining excellent course stability. On the premise of keeping the propeller speed unchanged, different control performance can be obtained by manually adjusting the performance parameter λ_ψ in the linear controller to meet different engineering requirements. It is worth mentioning that the ANFIS controller can rely on the strong learning ability of the neural network to control whether the desired course is a large course (ψ = 120°) or a small course (ψ = 60°), it can maintain course stability and improve energy efficiency, even in harsh sea conditions. This is achieved without the need to manually adjust parameters and has significant advantages over traditional linear control methods. Keeping the performance parameters and the environment unchanged, changing only the propeller speed can improve the control performance of the controller, and the maximum

steering angle does not change with the speed. The ANFIS-based course controller offers a promising ship course control scheme that strikes a balance between energy efficiency and control performance. Its adaptability and robustness make it suitable for engineering applications, with the potential to lead to safer, more economical, and environmentally friendly navigation practices.

Currently, our research focuses on the motion response performance of ships with three degrees of freedom. The number of degrees of freedom will be increased in the future to more accurately describe the motion of ships in complex sea conditions. Considering the coupling effect of wind, wave, current, and other environmental factors, the structure number of the controller and the accuracy of the model are further improved.

Author Contributions: Conceptualization, Y.G., R.Y., Z.Z. and B.H.; methodology, Y.G.; software, R.Y.; validation, Y.G. and R.Y.; formal analysis, R.Y.; investigation, B.H.; resources, Z.Z.; data curation, Y.G.; writing—original draft preparation, Y.G. and R.Y.; writing—review and editing, R.Y.; visualization, R.Y.; supervision, Z.Z.; project administration, Y.G.; funding acquisition, Y.G.; Z.Z. and B.H. All authors have read and agreed to the published version of the manuscript.

Funding: The present work was supported by the National Natural Science Foundation of China (Grant No. 52071200). We gratefully acknowledge the financial support of the Shanghai Commission of Science and Technology Project (Grant No. 23010501900).

Institutional Review Board Statement: Not applicable.

Informed Consent Statement: Not applicable.

Data Availability Statement: Data are contained within the article.

Conflicts of Interest: Author Bing Han is employed by Shanghai Ship and Shipping Research Institute, others declare no conflict of interest.

References

1. Liu, J.; Jiang, X.; Huang, W.; He, Y.; Yang, Z. A novel approach for navigational safety evaluation of inland waterway ships under uncertain environment. *Transp. Saf. Environ.* **2022**, *4*, tdab029. [CrossRef]
2. Kose, S.; Sekban, D.M. Emphasizing the importance of using cold-ironing technology by determining the share of hotelling emission value within the total emission. *Transp. Saf. Environ.* **2022**, *4*, tdac010. [CrossRef]
3. Chen, X.; Zheng, J.; Li, C.; Wu, B.; Wu, H.; Montewka, J. Maritime traffic situation awareness analysis via high-fidelity ship imaging trajectory. *Multimed. Tools Appl.* **2024**, *83*, 48907–48923. [CrossRef]
4. Sahal, M.; Gamayanti, N.; Cendikiarani, M.T. Surge Speed and Yaw Angle Control System Design on Unmanned Surface Vehicle (USV) Using PID-Fuzzy-Genetic Algorithm. In Proceedings of the 2024 International Seminar on Intelligent Technology and Its Applications (ISITIA), Mataram, Indonesia, 10–12 July 2024; IEEE: New York, NY, USA, 2024.
5. Xu, C.; Zhou, X.; Ren, H.; Sutulo, S.; Soares, C.G. Real-time simulation of ship overtake maneuvering at different water depths with a ship motion controller. *Ocean Eng.* **2024**, *311*, 119021. [CrossRef]
6. Bayezit, I.; Jambak, A.I.; Kinaci, O.K.; Fridan, B. Sensor data-based system identification and modular autopilot control instrumentation of marine craft. *Ocean Eng.* **2025**, *317*, 119793. [CrossRef]
7. Liu, L.; Zhang, L.; Pan, G.; Zhang, S. Robust yaw control of autonomous underwater vehicle based on fractional-order PID controller. *Ocean Eng.* **2022**, *257*, 111493. [CrossRef]
8. Suid, M.H.; Ahmad, M.A. Optimal tuning of sigmoid PID controller using Nonlinear Sine Cosine Algorithm for the Automatic Voltage Regulator system. *ISA Trans.* **2022**, *128*, 265–286. [CrossRef]
9. Tao, S.; Ju, Z.; Zhang, H.; Dong, X.; Chen, J. Path following of autonomous vehicles with an optimized brain emotional learning–based intelligent controller. *SAE Int. J. Connect. Autom. Veh.* **2023**, *6*, 241–250. [CrossRef]
10. Islam, M.M.; Siffat, S.A.; Ahmad, I.; Liaquat, M. Supertwisting and terminal sliding mode control of course keeping for ships by using particle swarm optimization. *Ocean Eng.* **2022**, *266*, 112942. [CrossRef]
11. Hosseinabadi, P.A.; Abadi, A.S.S.; Mekhilef, S. Fuzzy adaptive finite-time sliding mode controller for trajectory tracking of ship course systems with mismatched uncertainties. *Int. J. Autom. Control* **2022**, *16*, 255–271. [CrossRef]
12. Rezaei, A.; Tabatabaei, M. Ship roll stabilization using an adaptive fractional-order sliding mode controller. *Ocean Eng.* **2023**, *287*, 115883. [CrossRef]

13. Xu, Y.; Zhao, X.; Li, G. Design and analysis of 3-UPU wave compensation platform based on improved sliding mode control. *Ships Offshore Struct.* **2024**, *19*, 2040–2049. [CrossRef]
14. Chen, X.; Wu, H.; Han, B.; Liu, W.; Montewka, J.; Liu, R.W. Orientation-aware ship detection via a rotation feature decoupling supported deep learning approach. *Eng. Appl. Artif. Intell.* **2023**, *125*, 106686. [CrossRef]
15. Nasir, N.M.; Ghani, N.M.A.; Nasir, A.N.K.; Ahmad, M.A.; Tokhi, M.O. Neuro-modelling and fuzzy logic control of a two-wheeled wheelchair system. *J. Low Freq. Noise Vib. Act. Control* **2024**, 14613484241287608. [CrossRef]
16. Aghaseyedabdollah, M.; Abedi, M.; Pourgholi, M. Interval type-2 fuzzy sliding mode control for a cable-driven parallel robot with elastic cables using metaheuristic optimization methods. *Math. Comput. Simul.* **2024**, *218*, 435–461. [CrossRef]
17. Arifi, A.; Bouallègue, S. Takagi–Sugeno fuzzy-based approach for modeling and control of an activated sludge process. *Int. J. Dyn. Control* **2024**, *12*, 3123–3138. [CrossRef]
18. Han, B.; Duan, Z.; Peng, Z.; Chen, Y. A Ship Path Tracking Control Method Using a Fuzzy Control Integrated Line-of-Sight Guidance Law. *J. Mar. Sci. Eng.* **2024**, *12*, 586. [CrossRef]
19. Li, Y.; Song, G.; Yip, T.-L.; Yeo, G.-T. Fuzzy Logic-Based Decision-Making Method for Ultra-Large Ship Berthing Using Pilotage Data. *J. Mar. Sci. Eng.* **2024**, *12*, 717. [CrossRef]
20. Du, L.; Wu, Q.; Shu, Y.; Li, G. The effects of online-training artificial neural network mechanism and multi-stage parametric modeling method on simulation-based design system for ship optimization. *Ocean Eng.* **2024**, *309*, 118284. [CrossRef]
21. Unar, S.; Unar, A.M.; Memon, A.Z.; Narejo, S. A neural network-based heading and position control system of a ship. *Mehran Univ. Res. J. Eng. Technol.* **2022**, *41*, 172–177. [CrossRef]
22. Deraj, R.; Kumar, R.S.; Alam, M.S.; Somayajula, A. Deep reinforcement learning based controller for ship navigation. *Ocean Eng.* **2023**, *273*, 113937. [CrossRef]
23. Wakita, K.; Maki, A.; Umeda, N.; Miyauchi, Y.; Shimoji, T.; Rachman, D.M.; Akimoto, Y. On neural network identification for low-speed ship maneuvering model. *J. Mar. Sci. Technol.* **2022**, *27*, 772–785. [CrossRef]
24. Bouaiss, O.; Mechgoug, R.; TalebAhmed, A.; Brikel, A.E. Adaptive neural network-based compensation control of quadrotor for robust trajectory tracking. *Int. J. Adapt. Control Signal Process.* **2023**, *37*, 2772–2793. [CrossRef]
25. Zhao, Z.; Deng, L.; Yu, W.; Wang, C.; Wang, X.; Zhang, X. Adaptive Neural Event-Based Course-Keeping Control of Marine Vessel. In Proceedings of the 2024 Second International Conference on Cyber-Energy Systems and Intelligent Energy (ICCSIE), Shenyang, China, 17–19 May 2024; IEEE: New York, NY, USA, 2024; pp. 1–5.
26. Le, T.T. Ship heading control system using neural network. *J. Mar. Sci. Technol.* **2021**, *26*, 963–972. [CrossRef]
27. Karaboğa, D.; Kaya, E. Training ANFIS by using the artificial bee colony algorithm. *Turk. J. Electr. Eng. Comput. Sci.* **2017**, *25*, 1669–1679. [CrossRef]
28. Yasukawa, H.; Sakuno, R. Application of the MMG method for the prediction of steady sailing condition and course stability of a ship under external disturbances. *J. Mar. Sci. Technol.* **2020**, *25*, 196–220. [CrossRef]
29. Zhang, G. Calculation of Hydrodynamic Derivative of Ship Maneuverability Based on Numerical PMM Test. Ph.D. Thesis, Dalian Maritime University, Dalian, China, 2023.
30. Yasukawa, H.; Hirata, N.; Yamazaki, Y. Effect of bilge keels on maneuverability of a fine ship. *J. Mar. Sci. Technol.* **2018**, *23*, 302–318. [CrossRef]
31. Zhang, W.; Zou, Z.; Deng, D. A study on prediction of ship maneuvering in regular waves. *Ocean Eng.* **2017**, *137*, 367–381. [CrossRef]
32. Fossen, T.I. *Handbook of Marine Craft Hydrodynamics and Motion Control*; John Wiley & Sons: London, UK, 2011.
33. Yasukawa, H. Simulations of a ship maneuvering in waves. *J. Jpn. Soc. Nav. Archit. Ocean. Eng.* **2006**, *4*, 127–136. [CrossRef]
34. Zhang, Z.; Zou, Z.; Yang, J.; Zhang, X. Nonlinear hydrodynamic model-based course control and roll stabilization by taking rudder and propeller actions. *Ocean Eng.* **2022**, *263*, 112377. [CrossRef]

Disclaimer/Publisher's Note: The statements, opinions and data contained in all publications are solely those of the individual author(s) and contributor(s) and not of MDPI and/or the editor(s). MDPI and/or the editor(s) disclaim responsibility for any injury to people or property resulting from any ideas, methods, instructions or products referred to in the content.